Supplementary Information

for

Mechanical Metamaterials with Star-Shaped Pores exhibiting Negative and Zero Poisson's Ratio

LM, MM, KT, RG, DA, KEE, JNG*, JCT*

Table of Contents

1. Material Properties, Fabrication and Loading of the 3D Printed Prototypes

The resin used to produce the 3D printed prototypes was the Tough Resin of the Form2 Formlabs 3D Printer [32]. This resin was chosen due to its ability to withstand high stresses and strains before fracturing which should make it ideal to produce models which deform via localized hinging/flexural deformations.

The stress-strain behaviour of this material was found by testing three dog-bone shaped samples on a tensile loading machine. The dog-bones were constructed as shown in Figure S1. The dimensions of the dog-bones were as follows: w_{edge} = 10 mm, l_{edge} = 10 mm, w_{mid} = 5 mm, l_{mid} = 20 mm, r = 13.34 mm and d = 0.5 mm. The dog-bones were printed at an orientation of 45° to the printing surface using supports.

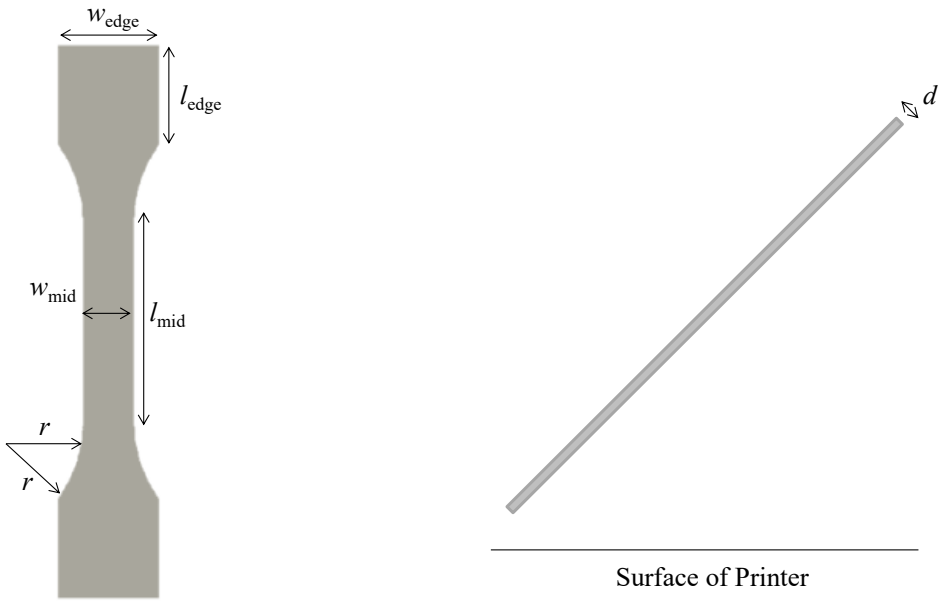

Figure S1: Diagram showing the dimensions and printing orientation of the dog-bones.

Following printing, the dog-bones were cured under UV light with a wavelength of 365 nm for 8 hours at room temperature and then subjected to tensile testing using a displacement rate of 1.5 mm/minute. A stress-strain graph was plotted from the force-extension data obtained (see Figure S2) and the Mooney-Rivlin 5-Parameter hyper-elastic model was fitted to the experimental data.

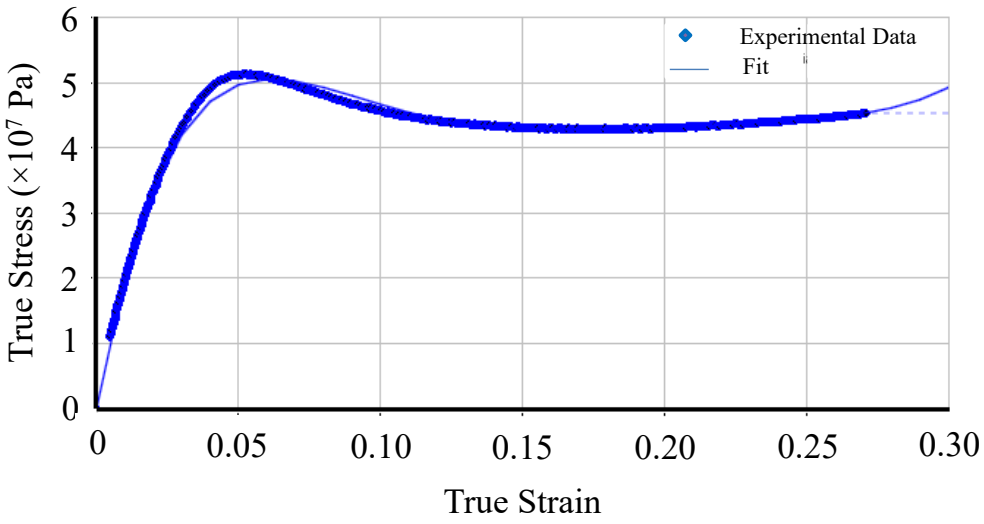

Figure S2: True stress-strain plots obtained from the dog-bones tested, fitted with a 5-parameter Mooney-Rivlin hyper-elastic model. The parameters used were as follows: C01 = 6.4962 × 10^9, C02 = 6.313 × 10^{10}, C10 = -6.1015 × 10^9, C11 = = -8.875 × 10^{10}, C20 = = 3.311 × 10^{10}, D1 = 0 (since material is assumed to be nearly incompressible).

The star perforation prototypes were printed and cured in the same conditions as the dog-bone test pieces described above. The final sample size, number of repeating units and dimensions of the perforations were chosen with the explicit aim of producing a model with the maximum permissible number of repeating units (to minimize the influence of edge effects on the repeating units in the centre of the sample from which the extension measurements were taken) while at the same time ensuring that the dimensions of the repeating units are not too small that defects arising from the 3D printer resolution play a significant role in the deformation of the final sample. In view of this, the following parameters were used:

a. Three-Star Perforated System (Figure S3a)
Gauge Length = 106 mm, Number of Horizontal Repeating Units = 6, Number of Vertical Repeating Units = 6, h = 8 mm, b = 3 mm, s = 1 mm, Depth = 10 mm

b. Four-Star Perforated System (Figure S3b)
Gauge Length = 107 mm, Number of Horizontal Repeating Units = 7, Number of Vertical Repeating Units = 8, h = 10 mm, b = 3 mm, s = 1 mm, Depth = 10 mm

c. Six-Star Perforated System (Figure S3c)
Gauge Length = 104 mm, Number of Horizontal Repeating Units = 6, Number of Vertical Repeating Units = 6, h = 10 mm, b = 3 mm, s = 1 mm, Depth = 10 mm

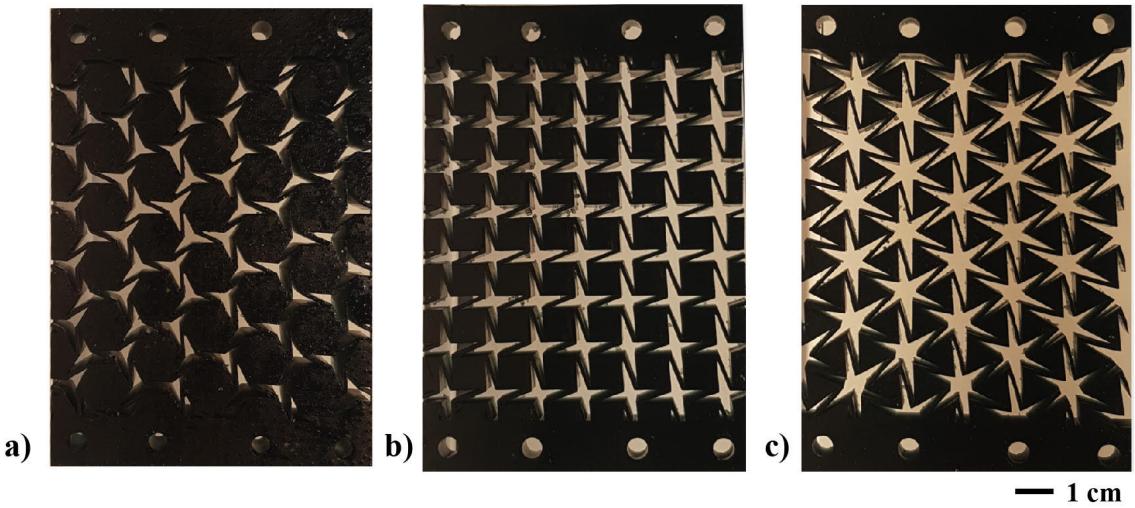

Figure S3: Pictures of the 3D printed (a) three-, (b) four- and (c) six-star perforated prototypes.

The 3D printed prototypes were loaded on a Testometric Tensile Loading machine. As shown in Figure S4, the samples were clamped from the edges using custom grips. A Messphysik video extensometer was used to record extension readings. The readings were taken from the centermost repeating units of the sample using the markers shown in Figure S4, where three measurements were taken for changes in the direction perpendicular to the loading direction and one measurement was taken for changes in the loading direction.

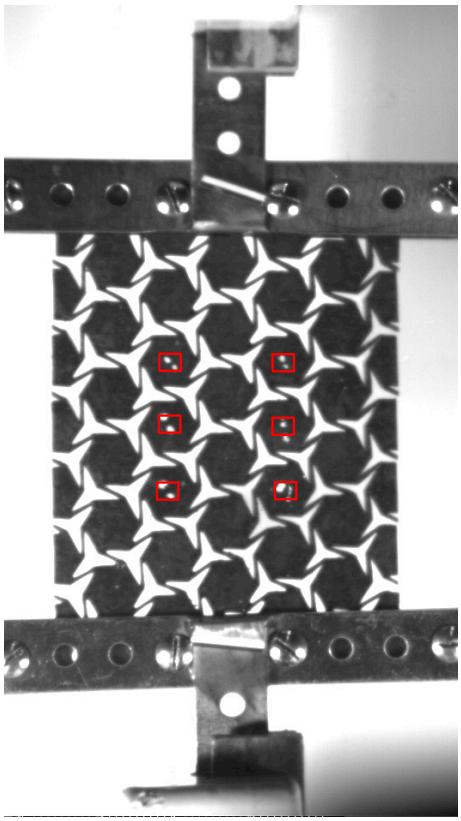

Figure S4: A clamped sample indicating the markers used to obtain extension readings.

These readings were then used to obtain the instantaneous Poisson's ratio, which was calculated from the differentials of a fourth-order polynomial curve fitted on a plot of the *x*-

and *y*-dimensions of the cell. This property is expected to provide a clearer picture of the changes in Poisson's ratio upon increasing strain, than the engineering or true Poisson's ratio, which are both subjected to bias from the initial Poisson's ratio of the sample. This method for measuring the Poisson's ratio has also been previously employed to study the high strain Poisson's ratio of graphene [5], tendons [10] and perforated systems [25], and a detailed description about its implementation may be found in Gatt *et al.* 2015 [10].

2. Linear Mechanical Properties of Tensile Loading in the *x*-direction

The plots shown below show the Poisson's ratios and effective Young's moduli obtained from the linear Finite Element simulations for loading in the *x*-direction. As one may observe, the values are nearly identical to those obtained from loading in the *y*-direction (see Figure 2 of the main manuscript).

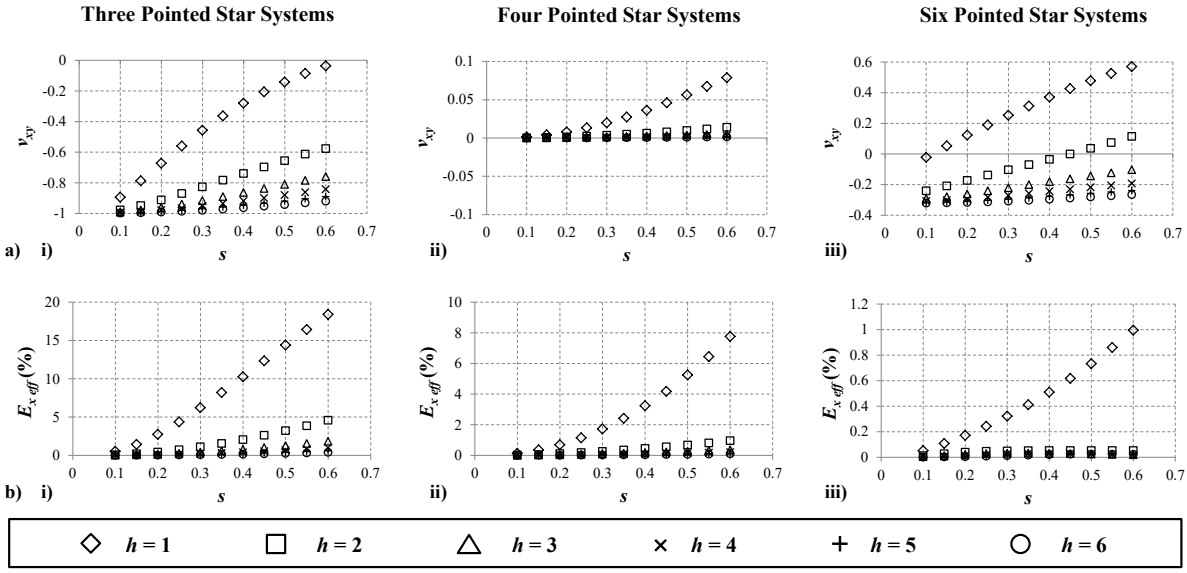

Figure S5: Plots showing the simulated on-axis a) Poisson's ratios, v_{yx}, and b) effective Young's moduli, $E_{y\,eff}$ (as a percentage of the material Young's modulus, E_{mat}) for the i) 3-star, ii) 4-star and iii) 6-star pore shaped systems for the application of a uniaxial load in the *x*-direction.

3. Stress-Strain Plots of Non-linear FE Simulations with Periodic Boundary Conditions

The plots below show the engineering stress-strain plots of the non-linear FE Simulations conducted using periodic boundary conditions.

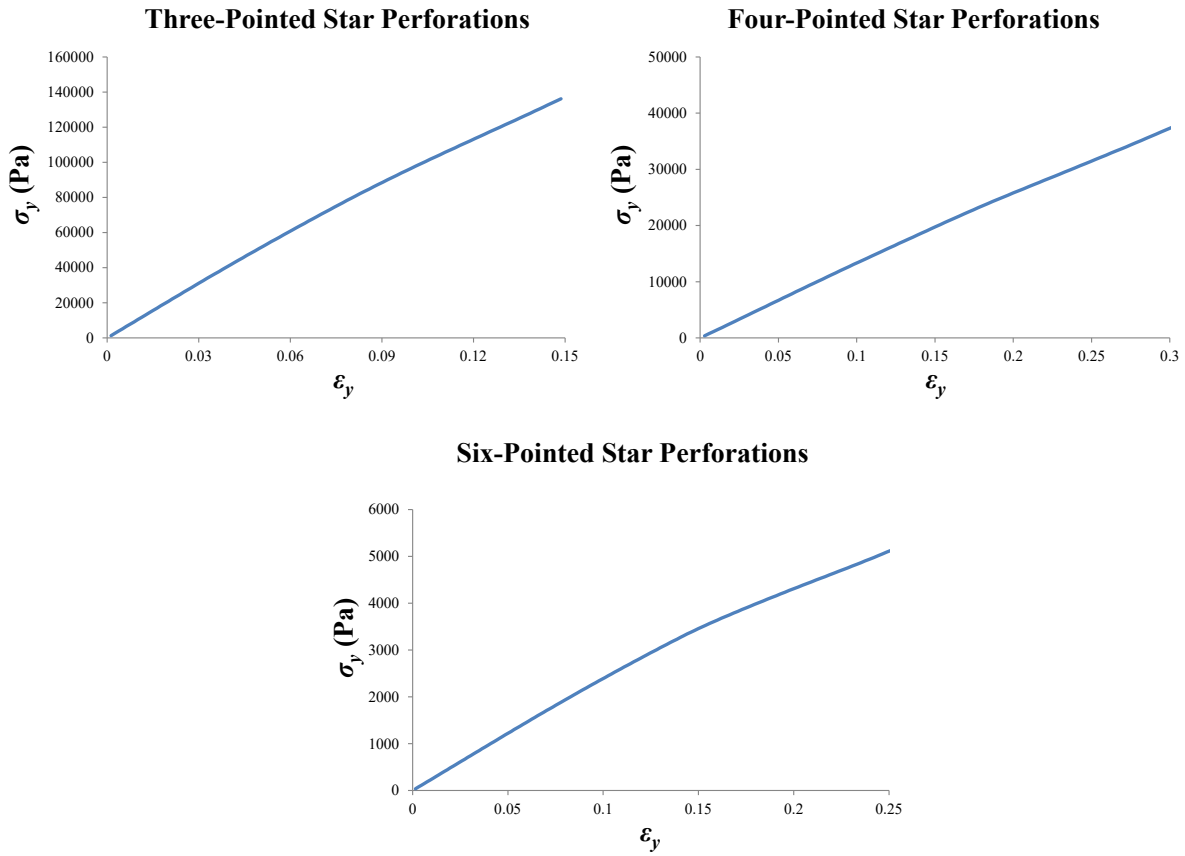

Figure S6: Plots showing the engineering stress-strain data obtained from the three systems simulated using Periodic Boundary Conditions using a non-linear analysis.